PNAS RESEARCH ARTICLE | MEDICAL SCIENCES

Acquired resistance to immunotherapy by physical barriers with cancer cell–expressing collagens in non–small cell lung cancer

Manli Wang[a,1], Yiyun Wang[b,1], Xiangyu Pan[b,1], Bo Wang[b,1], Yuying Wang[b,1], Xiangmeng Luo[b,1], Xiaofeng Deng[b], Li Liu[b], Xuelan Chen[b], Xiaoqian Zhai[b,c], Baohong Wu[b], Qi Zhang[b], Yifeng Ren[d,e], Jia Li[d], Xiaoyu Li[f], Fujun Cao[b], Yang Yang[b], Xintong Deng[b], Runhong Li[b], Zhenghao Lu[g], Ping Tan[b], Jingyao Chen[b], Yan Li[c], Yanyang Liu[c], Jiewei Liu[c], Yuan Wang[b], Hongxin Deng[b], Zhaoming Su[b], Weiya Wang[h], Yongsheng Wang[f], Shengyong Yang[b], Chengjian Zhao[b], Jianxin Xue[a], Yuquan Wei[b], Kang Zhang[i,2], Feifei Na[a,b,2], Yu Liu[b,j,2], and Chong Chen[a,b,k,l,2]

Affiliations are included on p. 10.

Edited by Gordon Freeman, Dana-Farber Cancer Institute, Boston, MA; received January 7, 2025; accepted May 1, 2025

Immunotherapy has become the standard treatment for many types of cancers, but an increasing number of patients who initially respond to these treatments develop acquired immunotherapy resistance (AIR). Here, we recapitulated the entire process of immunotherapy from response to AIR in mice with non–small cell lung cancer (NSCLC). With implanted tumor organoids derived from these models and serial transplants, we demonstrated that tumor cell–intrinsic mechanisms contributed significantly to AIR. Single-cell RNA sequencing and electron microscope assays revealed that resistant tumor cell–expressing collagens, including *Col3a1* and *Col6a1*, formed multiple physical barriers surrounding tumor cells. Disruption of these barriers by collagenase or knockout of both *Col3a1* and *Col6a1* in tumor cells could sensitize the tumors of AIR. Mechanistically, the TGFβ pathway was upregulated upon immunotherapy, and treatment with TGFβ significantly increased the expression levels of both *Col3a1* and *Col6a1* in tumor cells. COL3A1 formed a castle-like barrier for a cluster of tumor cells and prevented T cell infiltration, while COL6A1 formed an armor-like barrier surrounding individual tumor cells to protect them against direct T cell attack. Our data reveal a tumor cell–intrinsic mechanism of AIR, mediated by collagen-containing physical barriers, which immediately suggests a clinical treatment option.

NSCLC | immunotherapy | acquired resistance | collagens | physical barrier

Significance

The mechanisms underlying acquired immunotherapy resistance (AIR) are less understood. In this study, we generated non–small cell lung cancer (NSCLC) mouse models of AIR and found that tumor cell–expressing collagens, which formed physical barriers against T cell infiltration and attack, as a major tumor cell–intrinsic mechanism contributing to AIR. Genetically or pharmaceutically targeting these barriers could resensitize tumors for immunotherapy.

Cancer treatment has entered the era of immunotherapy (1). The immune checkpoint inhibitor (ICI) treatment itself or combined with other treatments is routine for most patients with more than 20 different types of cancers, including non–small cell lung cancer (NSCLC) (2–4). Despite the enthusiasm for these new treatments, resistance is very common to ICIs (5, 6). It is reported that about 60 to 80% of patients had no or little response to ICI treatment, which is called primary resistance. Previously, it was believed that immunotherapy should achieve a durable response, even a lasting cure for those who had an initial response, or in other terms, acquired resistance might be rare for immunotherapy (7, 8). However, with the increasingly widespread use of ICI, there is accumulating evidence indicating that cases with acquired resistance to ICIs are explosively observed in clinic (4, 9). For example, more than 65% of advanced NSCLC patients who achieved initial response to PD-1 blockade relapsed in 4 y (9, 10). To understand the mechanisms underlying acquired resistance is urgently needed to improve the outcomes of these patients.

The effect of immunotherapy can be affected by many factors, including both tumor cell–intrinsic and extrinsic features and the dynamic interactions of tumor cells and their microenvironment (5, 11–14). Evidence suggests that scarcity of potential tumor-suppressive immune cells, especially cytotoxic T cells, abundance of immunosuppressive Tregs, M2 macrophages, myeloid-derived suppressor cells, erythroid differentiated myeloid cells and cancer-associated fibroblasts, and various their secreted factors contribute to primary resistance to immunotherapy. In some types of cancers, patients with specific driver mutations, such as non–small cell lung cancer (NSCLC) with EGFR mutations, mutations in antigen-processing genes, MET amplification, and low tumor mutation burdens, have poor response to ICI treatment (15). Unfortunately, the mechanism of acquired resistance is significantly less studied. There are emerging data suggesting that patients who developed acquired resistance displayed diverse clinical and molecular features (4, 9). Loss of antigen presentation and activation of additional inhibitory checkpoints have been found in some

Author contributions: Yuquan Wei, K.Z., F.N., Yu Liu, and C.C. designed research; M.W., Yiyun Wang, X.P., Bo Wang, Yuying Wang, X. Luo, Xiaofeng Deng, L.L., Y.Y., Xintong Deng, R.L., Z.L., P.T., J.C., and Yan Li performed research; Baohong Wu, Q.Z., Y.R., J. Li, X. Li, F.C., Yanyang Liu, J. Liu, Yuan Wang, Z.S., W.W., Yongsheng Wang, C.Z., and J.X. contributed new reagents/analytic tools; X. Luo, X.C., X.Z., Xintong Deng, and H.D. analyzed data; and M.W., Yiyun Wang, X.P., Bo Wang, Yuying Wang, S.Y., and C.C. wrote the paper.

The authors declare no competing interest.

This article is a PNAS Direct Submission.

[1]M.W., Yiyun Wang, X.P., Bo Wang, Yuying Wang, and X. Luo contributed equally to this work.

[2]To whom correspondence may be addressed. Email: kang.zhang@gmail.com, nafeifei@foxmail.com, yuliuscu@scu.edu.cn, or chongchen@scu.edu.cn.

This article contains supporting information online at https://www.pnas.org/lookup/suppl/doi:10.1073/pnas.2500019122/-/DCSupplemental.

Published June 11, 2025.

patients, but more features associated with acquired resistance of immunotherapy need to be characterized. Among them, it is critical to identify the causal factors leading to acquired resistance and thus the corresponding solution for these patients.

In this study, we constructed a mouse model of NSCLC, the most common and lethal malignance for which ICI treatment has been incorporated into the first-line treatment paradigm, and recapitulated the features of patients through the full course of ICI treatment from responding to relapse and resistance. Through combined multiomics analyses and pathohistological assays, we found that during the process of acquired resistance, tumor cells expressed high levels of collagens, which built armor-like physical barriers and protected themselves from T cell attack. Disruption of these barriers could sensitize the tumors with acquired resistance to ICI treatment.

Results

Generating a Mouse Model of Lung Cancer with Acquired Immunotherapy Resistance (AIR). Animal models recapitulating the features of patients and feasible to be genetically engineered would be critical for investigating the molecular mechanisms of acquired resistance to immunotherapy. Therefore, we decided to create an "Organoid-initiated Precision Model" (OPCM) of NSCLC with a similar strategy which we have successfully applied for several other types of cancers (16–19). Briefly, epithelial organoids were cultured from the lung tissue of CGAS-Cas9-EGFP mice and then introduced with sg*Trp53*; *Kras*^{G12D}; *Myc*-luciferase (TKM). Once orthotopically transplanted into the lungs of the recipient mice, these implanted organoids developed into a single lesion in the lung, as indicated by the *Myc*-linked luciferase living image, micro-CT, and biopsy (Fig. 1 *A–E* and *SI Appendix*, Fig. S1*A*). Histopathological and transcriptome analyses indicated a diagnosis of NSCLC highly similar to human disease (20) (Fig. 1 *F* and *G*, *SI Appendix*, Fig. S1 *B–E*, and Datasets S1 and S2).

Then, these TKM mice were treated with vehicle or anti-PD1 antibody (Fig. 1*A*). These mice responded well to the treatment at the beginning, indicated by the significantly reduced bioluminescence signals. However, unfortunately, similar to many patients, most of the anti-PD1 antibody-treated mice relapsed after several rounds of treatments and eventually succumbed to the disease (Fig. 1 *H–J*). To validate the similarity of our mouse model to patients, we performed transcriptome analyses of sensitive and resistant tumors from mice and compared them with those of patients. The results showed that the up-regulated and down-regulated gene signatures in NSCLC patients with immunotherapy resistance were significantly positive and negative, respectively, in our mouse model of AIR (21) (*SI Appendix*, Fig. S1*F* and Datasets S3 and S4). Further, the resistance gene signature identified in our mouse model could predict the prognosis of NSCLC patients for ICI treatment in multiple cohorts (*SI Appendix*, Fig. S1*G* and Datasets S5 and S6). Thus, our mouse model of AIR faithfully represented the treatment course and molecular features of patients. To investigate whether the acquired resistance was tumor cell intrinsic or extrinsic, the implanted tumor organoids from the vehicle-treated (sensitive, Sen) and anti-PD1 antibody-treated (resistant, Res) tumors were transplanted into the secondary recipients, followed with further anti-PD1 antibody treatment (Fig. 1*K*). While the sensitive tumors were significantly repressed by the treatment, the resistant tumors kept growing (Fig. 1 *L* and *M*). Further, we cocultured the ovalbumin (OVA)-sensitive and OVA-resistant tumor organoids with activated cytotoxic OT-1 T cells and found that the survival rate of resistant tumor cells was significantly higher than the sensitive ones (*SI Appendix*, Fig. S2 *A* and *B*). These data strongly suggested that the AIR was mostly contributed by tumor-cell intrinsic mechanisms. Consistently, there were significantly fewer T cells infiltrated in the secondary transplanted resistant tumors, with or without anti-PD1 antibody treatment, compared to the sensitive tumors (22, 23) (*SI Appendix*, Fig. S2 *C–F*). To further confirm the effect of resistant tumors on T cell infiltration, sensitive and resistant implanted tumor organoids with OVA were subcutaneously transplanted into nude mice, followed by tail vein injection of OT-1 CD8$^+$ T cells. Significantly fewer T cells were identified in the OVA-resistant tumors than in the sensitive tumors (*SI Appendix*, Fig. S2 *G–I*). Thus, the resistant tumor cells could prevent the infiltration and killing of cytotoxic T cells through a tumor cell–intrinsic mechanism independent of antigens.

Self-Built Collagen Layers Are Associated with Tumor Cell–Intrinsic AIR. We next went further to identify the differences between the sensitive and resistant tumors. Hematoxylin and Eosin (H/E) staining showed that the resistant tumors lost the typical morphology of alveolar-like structures and acquired mesenchymal-like characteristics, indicated by composing of spindle cells arranged in poorly defined fascicles (Fig. 2*A*). Tumor organoids derived from the resistant tumors also displayed different morphology from those of sensitive ones (Fig. 2 *B* and *C*). To decipher the molecular characteristics of tumors with AIR, we performed multiomics analyses. Single-cell RNA sequencing (scRNA-seq) revealed dramatic changes in the cellular components of the resistant tumors compared to those of the sensitive ones. Most notable were the increased percentages of tumor cells and decreased percentages of T cells, which were further confirmed by spatial transcriptomics analyses and consistent with the above histopathological assays (Fig. 2*D*, *SI Appendix*, Fig. S3 *A–C*, and Datasets S7 and S8). Additionally, the T cells in the resistant tumors expressed significantly lower levels of markers of the early activation T cells and the effector memory T cells, both of which might be critical for ICI treatment (*SI Appendix*, Fig. S3*D* and Dataset S9). Pathway enrichment analysis of tumor cells revealed that genes highly expressed in resistant tumor cells were enriched in immunosuppression related pathways such as the TGFβ signaling pathway and Myc target pathways (24, 25) (Fig. 2*E*). Interestingly, we found that both RNA-seq and proteomics analysis of the sensitive and resistant implanted tumor organoids showed collagens and collagen-assemble-related genes were highly expressed in the tumor cells with AIR (Fig. 2*F* and Datasets S4 and S10). Consistently, collagen fibril structure and extracellular matrix (ECM) formation–related pathways were significantly positively enriched in the resistant tumors in mice and also in NSCLC patients refractory to ICI treatment (*SI Appendix*, Fig. S4*A* and Datasets S11 and S12). Among these collagen genes, *Col3a1* and *Col6a1* were most differently expressed in the resistant tumors (*SI Appendix*, Fig. S4*B*). qRT-PCR and western blotting confirmed the upregulation of *Col3a1* and *Col6a1* in the resistant tumor cells (*SI Appendix*, Fig. S4 *C* and *D*). The spatial transcriptomics data also showed that *Col3a1* and *Col6a1* were evenly distributed in the resistant tumor cells (*SI Appendix*, Fig. S4 *E* and *F*). And scRNA-seq analyses revealed that *Col3a1* and *Col6a1* were absent in the sensitive tumor cells but highly expressed in all the resistant tumor cells to levels similar to that in cancer-associated fibroblasts (CAFs) (Fig. 2*G* and *SI Appendix*, Fig. S4*G*).

To elucidate how these collagens upregulated in tumor cells with AIR, we found that the TGFβ pathway was significantly positively enriched in resistant tumors, and both *Tgfb1, Tgfbr1, Smad2, Smad4* were upregulated in the resistant tumor cells compared to the sensitive ones (Fig. 2 *E* and *H* and *SI Appendix*, Fig. S4 *H* and *I*). We further explored the potential mechanism how the TGFβ pathway was upregulated in tumor cells. We observed the upregulation of the TNFα signaling pathway in the tumor cells along

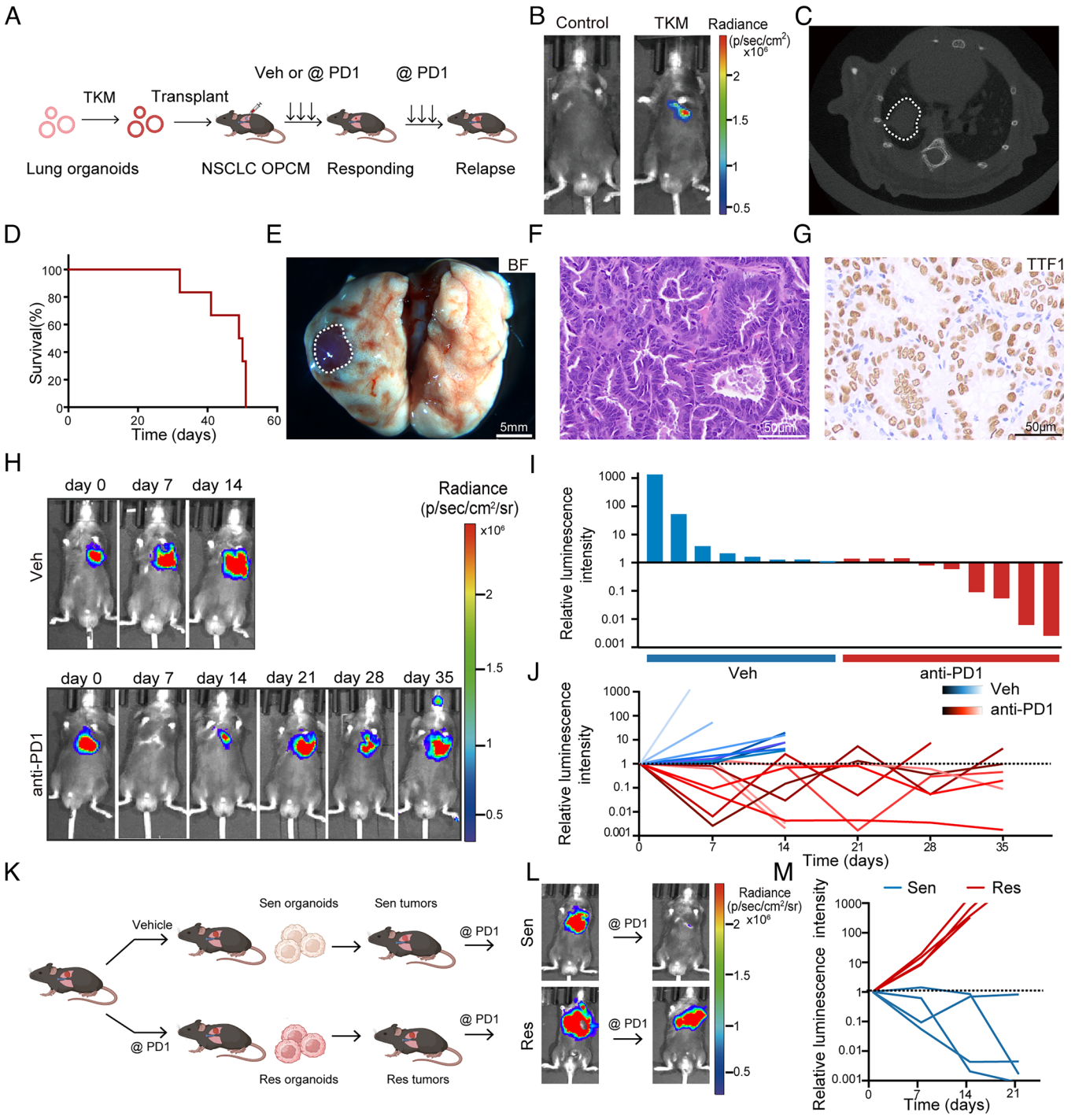

Fig. 1. Mimicking AIR of lung cancer in mice. (*A*) Schematic of the organoid-based strategy for generating an immunotherapy-resistant NSCLC mouse model. (*B*) Representative bioluminescence images of control (*Left*) and recipient mice (*Right*) transplanted with sg*Trp53*; *Kras*^{G12D}; and *Myc* (TKM) premalignant lung organoids at 25 d after transplantation (n = 6 mice). (*C*) Representative micro-CT image of TKM-recipient mice (n = 6 mice). (*D*) The survival curve of C57BL/6 mice orthotopically transplanted with TKM implanted organoids (n = 6 mice). (*E*) Representative bright-field image of the lungs of TKM-recipient mice (n = 6 mice). (Scale bar, 5 mm.) (*F*) Representative H/E staining images of TKM tumors (n = 6 mice). (Scale bar, 50 μm.) (*G*) Representative TTF1 IHC staining images of TKM tumors (n = 6 mice). (Scale bar, 50 μm.) (*H*) Representative bioluminescence images of TKM mice treated with vehicle (veh, *Upper*) or anti-PD1 antibody (anti-PD1, *Bottom*) once per week (n = 8 mice for veh and n = 9 mice for anti-PD1). (*I*) The waterfall plots showing the relative luminescence intensity of day 7 related to day 0 of TKM mice treated with vehicle or anti-PD1 treatment (n = 8 mice for veh and n = 9 mice for anti-PD1). (*J*) Curves showing the relative luminescence intensity related to day 0 of TKM mice treated with vehicle or anti-PD1 once per week. (*K*) Schematic of the second transplant of sensitive or resistant tumor cells and ICI treatment. (*L*) Representative bioluminescence images of sensitive (Sen) or resistant (Res) tumors treated with vehicle or anti-PD1 (n = 4 mice). (*M*) Curves showing the relative luminescence intensity related to day 0 of sensitive and resistant tumors after anti-PD1 treatment (n = 4 mice per group).

the resistance trajectory (Fig. 2*E*) and also noticed that the expressions of *Tnfrsf1a* and *TNF* were significantly increased in the resistant tumor cells and macrophages, respectively, compared to the sensitive ones (*SI Appendix*, Fig. S4 *J* and *K*). We proposed that macrophage-derived TNFα detected by resistant tumor cells expressing high levels of TNF receptor triggers *Tgfb1* expression in tumor cells. And the autocrine Tgfb1 could further upregulate the expressions of collagens. To investigate this further, we assessed the role of the TGFβ pathway in collagen regulation, sensitive tumor cells were incubated with varying concentrations of

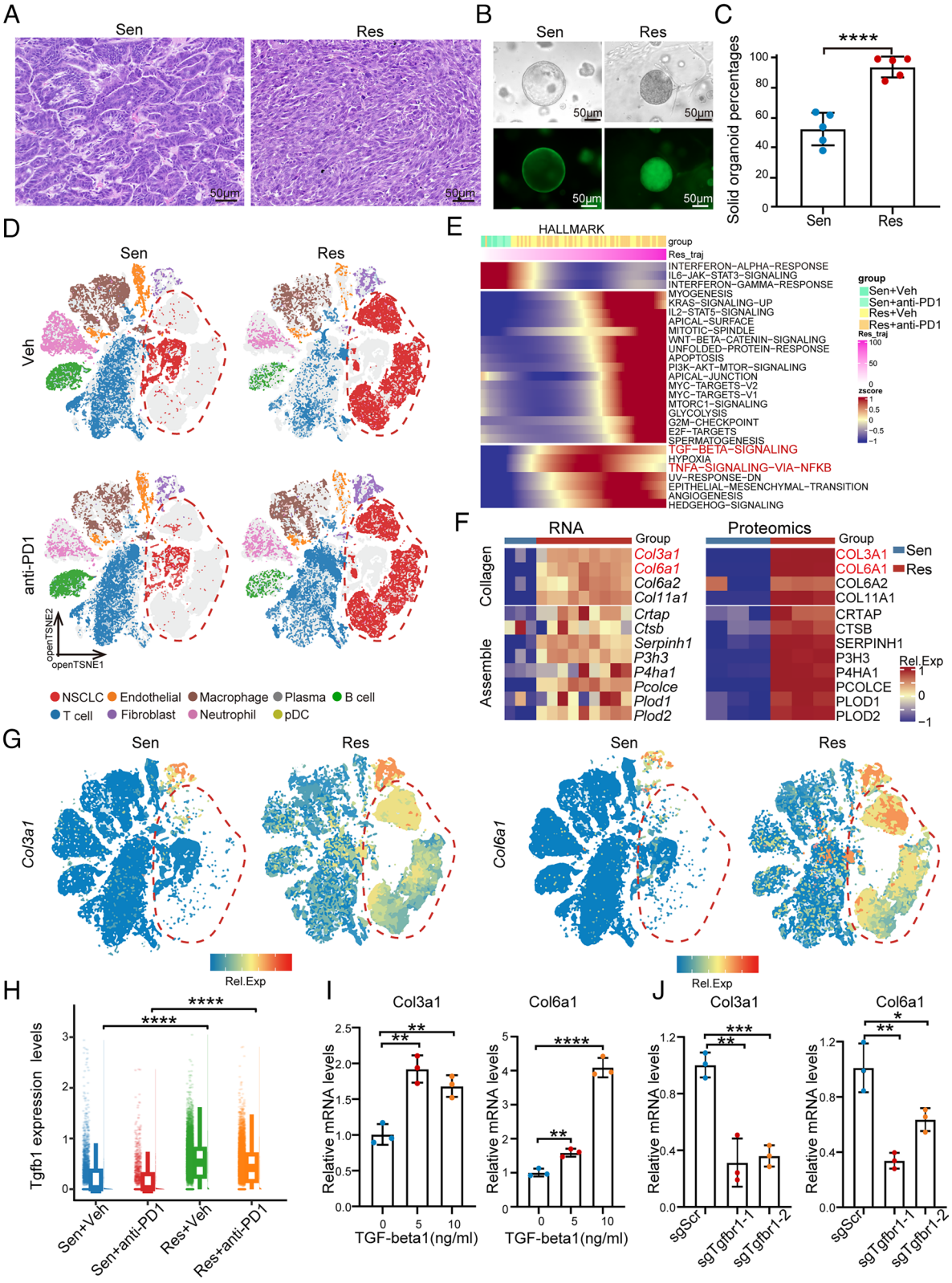

Fig. 2. The features of NSCLC with tumor cell–intrinsic resistance to immunotherapy. (*A*) Representative H/E staining images of Sen and Res tumors (n = 4 mice). (Scale bar, 50 μm.) (*B*) Representative bright-field and fluorescent images of implanted organoids generated from Sen and Res tumors (n = 4 mice). (Scale bar, 50 μm.) (*C*) The bar graphs showing the percentages of solid organoids in Sen and Res implanted tumor organoids (n = 5 independent sections). Data presented as mean ± SD. (*D*) Open t-distributed stochastic neighbor embedding (openTSNE) analysis of scRNA-seq data from Sen and Res tumors treated with Veh or anti-PD1. Dots represent individual cells, and colors represent different cell subtypes. (*E*) The heatmap displays HALLMARK-related gene set enrichment variation scores across the trajectory from sensitive to resistant tumor. (*F*) Heatmaps showing the collagen and collagen-assembly related genes highly expressed in resistant implanted organoids at RNA and proteomic levels. (*G*) OpenTSNE plots of expression distributions of *Col3a1* and *Col6a1* in Sen and Res tumors. (*H*) *Tgfb1* expression levels of tumor cells in sensitive and resistant tumors treated with Veh or anti-PD1. Wilcoxon signed-rank test. (*I*) The relative mRNA levels of *Col3a1* and *Col6a1* of resistant implanted tumor organoids with TGF-beta1 (n = 3 technical replicates). (*J*) The relative mRNA levels of *Col3a1* and *Col6a1* of resistant (Res) implanted tumor organoids with sg*Scr*, sg*Tgfbr1-1*, or sg*Tgfbr1-2* (n = 3 technical replicates). Data presented as mean ± SD. *P* values were calculated using two-tailed Student's *t* test (*C*, *I*, and *J*). ****$P < 0.0001$; ***$P < 0.001$; **$P < 0.01$; *$P < 0.05$.

TGF-beta1. qPCR and immunofluorescence stainings (IF) demonstrated that both the RNA and protein levels of COL3A1 and COL6A1 were significantly upregulated following TGF-beta1 stimulation (Fig. 2*I* and *SI Appendix*, Fig. S4 *L–N*). Consistently, *Tgfbr1* knockout in resistant tumor cells significantly decreased the expression of *Col3a1* and *Col6a1* (Fig. 2*J*). These findings suggest that the TGFβ pathway may be a key regulator of collagen formation in tumor cells with AIR.

We next confirmed the expression pattern of COL3A1 and COL6A1 in sensitive and resistant tumors. IF staining data showed that COL3A1 and COL6A1 were exclusively expressed by CAFs but not tumor cells in the sensitive tumors. In contrast, in the resistant tumors, COL3A1 and COL6A1 were mostly expressed by tumor cells (Fig. 3*A*). Second harmonic generation (SHG) microscopy revealed that collagen fibrils were enriched in the whole area in the resistant tumors but rare and limited to stromal regions in the sensitive tumors (Fig. 3*B*). To directly view the fibrils in the resistant tumors, we performed transmission electron microscope (TEM) and scanning electron microscope (SEM). The TEM assay showed that collagen fibrils formed an intact layer outside of each resistant tumor cell but invisible for the sensitive tumor cells (Fig. 3*C*). The SEM assay also revealed visualized collagen fibrils entirely covering all the resistant tumor cells, which were completely absent on the sensitive tumor cells (Fig. 3*D*). Thus, we revealed the physical barriers formed by tumor cell–expressing collagens for tumor cells with AIR.

Disruption of Collagen Layers Reduces AIR. Given the potential roles of these collagen-forming physical barriers in AIR, we explored whether the disruption of these barriers can overcome the resistance. We treated the resistant tumors in C57BL/6 mice with collagenase I, which could specifically digest collagens, together with anti-PD1 antibody (Fig. 4*A*). Collagenase treatment significantly decreased the growth of the resistant tumors (Fig. 4*B* and *SI Appendix*, Fig. S5*A*). The histological assay showed that there was a significantly increased area of necroptotic cells in the collagenase-treated tumors than the vehicle-treated ones (*SI Appendix*, Fig. S5*B*). Multiple IHC staining showed that the levels of COL3A1 and COL6A1 were reduced by collagenase treatment (Fig. 4*C*). Consistently, the collagen fibrils were significantly removed in the treated tumors, demonstrated by the

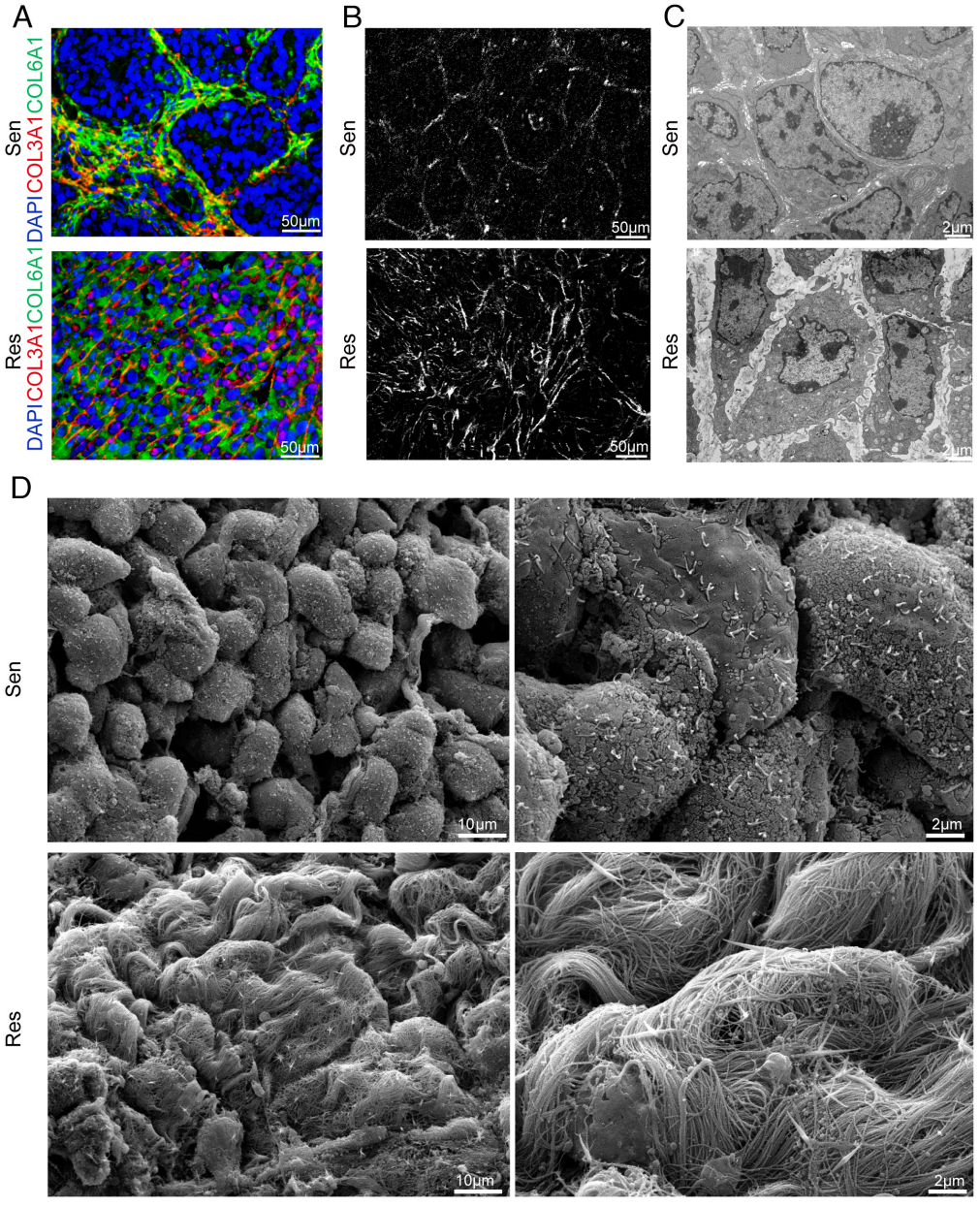

Fig. 3. Self-built collagen layers are associated with tumor cell–intrinsic AIR. (*A*) Representative COL3A1 and COL6A1 staining images of Sen and Res tumors (n = 4 mice). (Scale bar, 50 μm.) (*B*) Representative SHG microscopy images of Sen and Res tumors (representative of n = 4 mice). (Scale bar, 50 μm.) (*C*) Representative TEM images of Sen and Res tumors (representative of n = 4 mice). (Scale bar, 2 μm.) (*D*) Representative SEM images of Sen and Res tumors (representative of n = 4 mice). [Scale bars, 10 μm (*Left*), 2 μm (*Right*).]

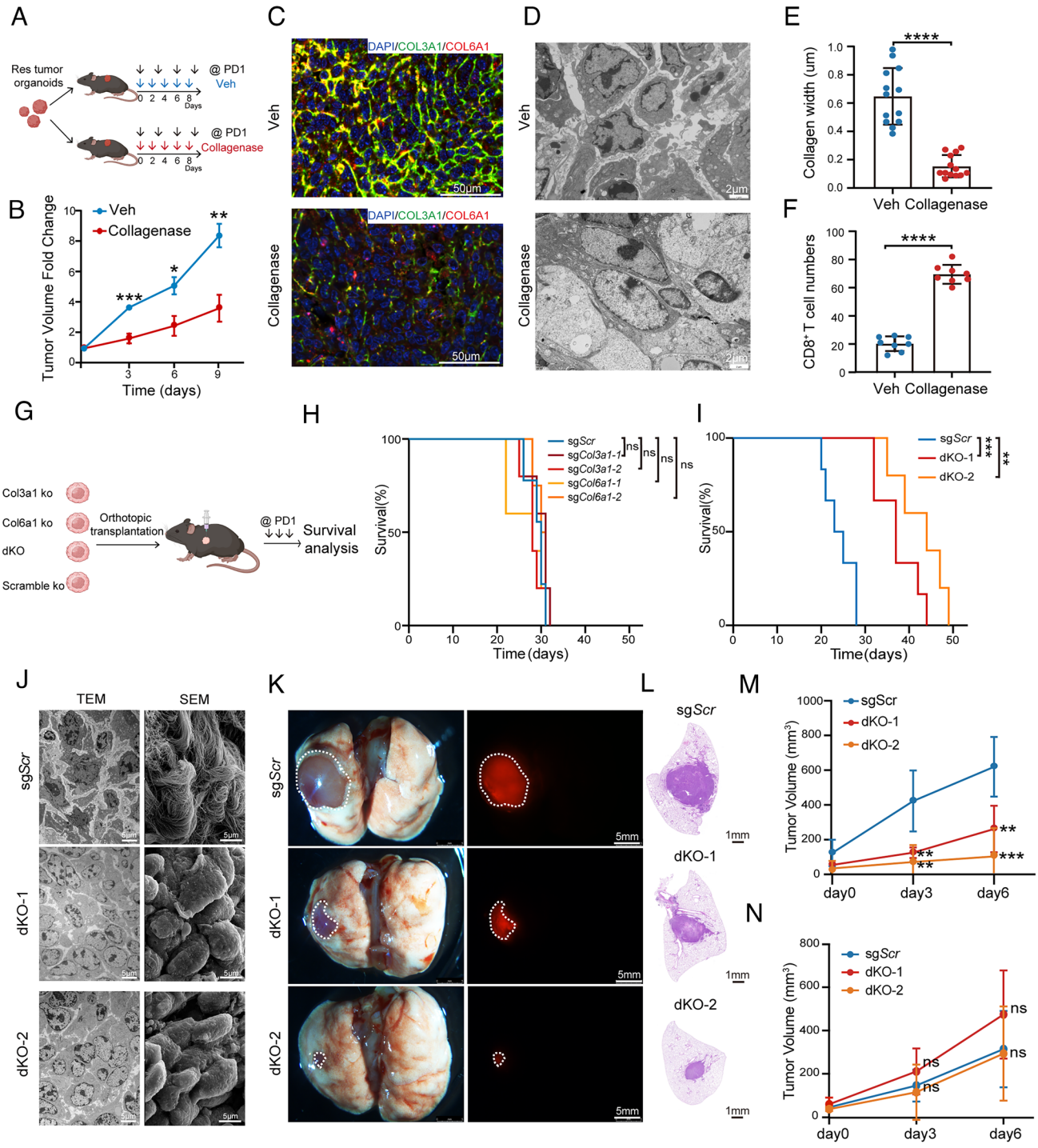

Fig. 4. Disruption of collagen layers reduces AIR. (*A*) Schematic of resistant tumors treated with anti-PD1 + vehicle or anti-PD1 + collagenase. (*B*) Curves showing the tumor volume fold changes related to day 0 of resistant tumors treated with anti-PD1 + vehicle or anti-PD1 + collagenase (n = 5 mice). Data presented as mean ± SEM. (*C*) Representative COL3A1 and COL6A1 staining images of resistant tumors treated with anti-PD1 + vehicle or anti-PD1 + collagenase (n = 3 mice per group). (Scale bar, 50 μm.) (*D*) Representative TEM images of resistant tumors treated with anti-PD1 + vehicle or anti-PD1 + collagenase (n = 3 mice per group). (Scale bar, 2 μm.) (*E*) Collagen width analysis of resistant tumors treated with anti-PD1 + vehicle or anti-PD1 + collagenase (independent sections of n = 3 mice). Data presented as mean ± SD. (*F*) Quantification of $CD8^+$ T cell numbers of resistant tumors treated with anti-PD1 + vehicle or anti-PD1 + collagenase (independent sections of n = 3 mice). Data presented as mean ± SD. (*G*) Schematic of the treatment of anti-PD1 in tumor cells with *Col3a1* or *Col6a1* single knockout or double knockout. (*H*) The survival curve of C57BL/6 mice orthotopically transplanted with resistant implanted tumor organoids with sg*Scr*, sg*Col3a1-1/2,* or sg*Col6a1-1/2* treated with anti-PD1 (n = 4-5 mice). (*I*) Survival curve of C57BL/6 mice orthotopically transplanted with resistant implanted tumor organoids with sg*Scr*, sg*Col3a1*+*Col6a1-1* (dKO-1), or sg*Col3a1*+*Col6a1-2* (dKO-2) resistant implanted tumor organoids treated with anti-PD1 (n = 5-6 mice). (*J*) Representative images of TEM (*Left*) and SEM (*Right*) of nude mice subcutaneously transplanted with resistant implanted tumor organoids with sg*Scr*, dKO-1, or dKO-2. (Scale bar, 5 μm.) (*K*) Representative bright-field & fluorescent images of the lungs of a recipient orthotopically transplanted with resistant implanted tumor organoids with sg*Scr*, dKO-1, or dKO-2 (representative of n = 5 mice). (Scale bar, 5 mm.) (*L*) H/E staining images (representative of n = 5 mice) of the lungs of a recipient orthotopically transplanted with resistant implanted tumor organoids with sg*Scr*, dKO-1, or dKO-2. (Scale bar, 1 mm.) (*M*) Curves showing the tumor volumes of C57BL/6 that subcutaneously transplanted with resistant implanted tumor organoids with sg*Scr*, dKO-1, or dKO-2 (n = 5 mice). Data presented as mean ± SD. (*N*) Curve showing the tumor volumes of nude mice that subcutaneously transplanted with resistant implanted tumor organoids with sg*Scr*, dKO-1, or dKO-2 (n = 5 mice). Data presented as mean ± SD. *P* values were calculated using two-tailed Student's *t* test (*B*, *E*, *F*, *M*, and *N*). ****$P < 0.0001$; ***$P < 0.001$; **$P < 0.01$; *$P < 0.05$; ns, not significant.

TEM assay (Fig. 4 *D* and *E*). Since collagenase could not penetrate the intact cells, these results confirmed that these collagens and the fibrils formed by them were mostly in the ECM of the resistant tumor cells. In addition, we found that there were significantly more infiltration of T cells in the collagenase-treated tumors than in the vehicle-treated ones, which indicated that collagens may form physical barriers in AIR to prevent T cell infiltration (Fig. 4*F* and *SI Appendix*, Fig. S5*C*). To further explore the functional roles of these collagen-forming physical barriers in immunotherapy resistance, we disrupted the upregulated collagen genes *Col3a1, Col6a1, Col6a2, Col6a3, Col11a1,* and *Col12a1* together in the resistant tumor cells by CRISPR/Cas9 and tested their sensitivity to anti-PD1 (*SI Appendix*, Fig. S5*D*). The data showed that loss of these collagen genes significantly extended the survival of the recipient mice, indicating their function in promoting resistance to immunotherapy (*SI Appendix*, Fig. S5*E*). Among all collagens, we checked the function of the most upregulated genes *Col3a1*, *Col6a1* individually and in combination in AIR (Fig. 4*G*). Disruption of *Col3a1* or *Col6a1* in the resistant tumor cells had a minimal effect on the growth of the resistant tumor organoids in vitro (*SI Appendix*, Fig. S5 *F* and *G*). Also, single knockout of these collagens had minimal effects on the response of the AIR tumors to anti-PD1 antibody treatment in vivo (Fig. 4*H* and *SI Appendix*, Fig. S5 *H* and *I*). H/E stainings showed that *Col3a1* or *Col6a1* disruption itself partially reversed the pathology of tumors with AIR (*SI Appendix*, Fig. S5*J*). On the contrary, double-knockout *Col3a1* and *Col6a1* (dKO) significantly extended the survival of mice with resistant tumors upon anti-PD1 antibody treatment, compared to those with *sgScr* tumors (Fig. 4*I*). TEM assays revealed that dKO completely removed the collagen fibrils on the surface of the resistant tumor cells, which suggested that COLl3A1 and COL6A1 were the major components of collagen fibrils (Fig. 4*J*). Consistently, the biopsy showed that dKO tumors were significantly smaller than the control tumors (Fig. 4 *K* and *L*). H/E staining showed that dKO also reversed the histological feature of the resistant tumors (*SI Appendix*, Fig. S5*K*). We next implanted either the control or dKO tumors into both immunocompetent and immunodeficient mice. ICI treatment significantly repressed the growth of dKO tumors than control ones in immunocompetent mice. However, it had a minimal significant effect on the growth of either dKO or control tumors in immunodeficient mice (Fig. 4 *M* and *N*). To further validate whether *Col3a1* and *Col6a1* were the most important collagens responsible for AIR, we treated the dKO OVA-expressing resistant tumor cells with vehicle or collagenase and then cocultured them with OT-1 T cells (*SI Appendix*, Fig. S5*L*). The results showed that collagenase treatment did not have an additional effect on the survival of these tumor cells, compared to the dKO tumor cells treated with vehicle (*SI Appendix*, Fig. S5 *M* and *N*). Further, we performed an in vivo experiment to compare the efficacy of anti-PD1 antibody treatment on dKO tumors with or without collagenase treatment combination (*SI Appendix*, Fig. S5*O*). Consistent with the in vitro killing experiment, there was no significant difference between dKO + vehicle and dKO + collagenase (*SI Appendix*, Fig. S5*P*). Histology analyses showed that both dKO tumors treated with and without collagenase had similar massive necrosis, suggesting response to anti-PD1 treatment (*SI Appendix*, Fig. S5*Q*). Taken together, these data suggest that *Col3a1* and *Col6a1* are the major collagens responsible for AIR and that disruption of collagen layers may reverse AIR in a manner dependent on T cell function.

Col3a1 and Col6a1 Prevent T Cell Infiltration and Killing, Respectively. To understand the mechanisms leading to the different results between single knockouts of either *Col3a1* or *Col6a1* and the double knockout of *Col3a1* and *Col6a1*, we further examined the roles of *Col3a1* and *Col6a1* in AIR. Interestingly, using multiple IHC staining, we found that COL3A1 formed a castle-like structure surrounding clusters of several tumor cells and COL6A1 created an armor-like structure around each tumor cell (Fig. 5*A*). We proposed that these collagen layers might function as physical barriers against attack by immune cells, especially cytotoxic T cells. Intriguingly, multiple IHC staining revealed that tumors with *Col3a1* loss had significantly increased infiltrated T cells, while those with *Col6a1* deficiency were similar to the control tumors (Fig. 5*B* and *SI Appendix*, Fig. S6 *A–C*). These data suggest that the castle-like barrier, formed by COL3A1, is essential for restraining T cell infiltration.

To test their roles in direct T cell killing, we cocultured OVA-expressing resistant tumor cells with or without collagen knockout with activated $CD8^+$ OT-1 T cells. The results demonstrated that sg*Col6a1* tumor cells had significantly less survival rate than those with sg*Scr* while *Col3a1* deficiency did not affect the cytotoxic killing by T cells in vitro, dKO further sensitized the OT-1 T cell killing of OVA-resistant tumor cells in vitro. These observations suggested that the armor-like barrier, consisting of COL6A1, could protect the tumor cells from T cell killing (Fig. 5 *C–E*). Furthermore, dKO significantly increased T cell infiltration in both C57BL/6 recipient mice and nude mice transplanted with OVA-resistant tumors and OT-1 T cells (Fig. 5 *F* and *G* and *SI Appendix*, Fig. S6 *D–G*). And taken together, multiple collagen-forming physical barriers contributed to AIR by preventing T cell infiltration and killing. The gene signature associated with immunotherapy resistance in NSCLC patients was significantly upregulated in the resistant tumor cells compared to the sensitive ones, but significantly downregulated by dKO (*SI Appendix*, Fig. S7 *A–C*). Consistent with the proposed physical barriers of *Col3a1* and *Col6a1* against T cell infiltration and killing, there were significantly increased early activated and effector/memory $CD8^+$ T cells in the dKO tumors (*SI Appendix*, Fig. S7*D*). And the cytotoxic T cells in the dKO tumors also expressed higher expression levels of *Gzmb* and *Gzmk*, the key effector genes for T cell killing, compared to those in the control tumors (*SI Appendix*, Fig. S7*E*).

Collagen Layers Are Associated with AIR in Patients. In the end, we validated the clinical relevance of the collagen-formed physical barrier mechanism of AIR in patients. Multiple collagen genes, including *COL3A1* and *COL6A1*, were highly expressed in NSCLC patients who were resistant to ICI expressed, compared to the responsive ones (10, 21) (Fig. 6*A*, *SI Appendix*, Fig. S8*A*, and Dataset S13). And multiomics pathway analyses showed that the collagen pathways were not only significantly enriched in mouse tumors with AIR but also in patients who were resistant to ICI at all the epigenetic, transcriptomic, and proteomic levels (*SI Appendix*, Fig. S8*B*). In NSCLC patients, the expression levels of *COL3A1* and *COL6A1* were significantly positively associated with the immunotherapy resistance gene signature in patients (*SI Appendix*, Fig. S8*C*). Importantly, the high levels of *COL3A1* and *COL6A1* were significantly associated with poor prognosis of NSCLC patients treated with immunotherapy in multiple cohorts (21, 26–28) (Fig. 6*B* and Dataset S5, S6 and S14).

Then, we collected samples of 12 NSCLC patients without ICI treatment and 15 ones with acquired resistance to anti-PD1 antibody treatment. Multiple IHC stainings showed that 6 patients were COL3A1 and COL6A1 double positive in the tumor cells, and 1 and 3 were COL3A1 or COL6A, respectively, single positive in the acquired resistant group. In contrast, in the naïve group, only 2 were COL3A1 positive, and none of them was double positive (Fig. 6 *C* and *D* and Dataset S15). Furthermore, the T cell infiltration was also higher in $collagen^{high}$ ones than that in $collagen^{low}$ samples (Fig. 6*E*). In the recently published MSKCC cohort of NSCLC patients with acquired resistance to anti-PD1 antibody

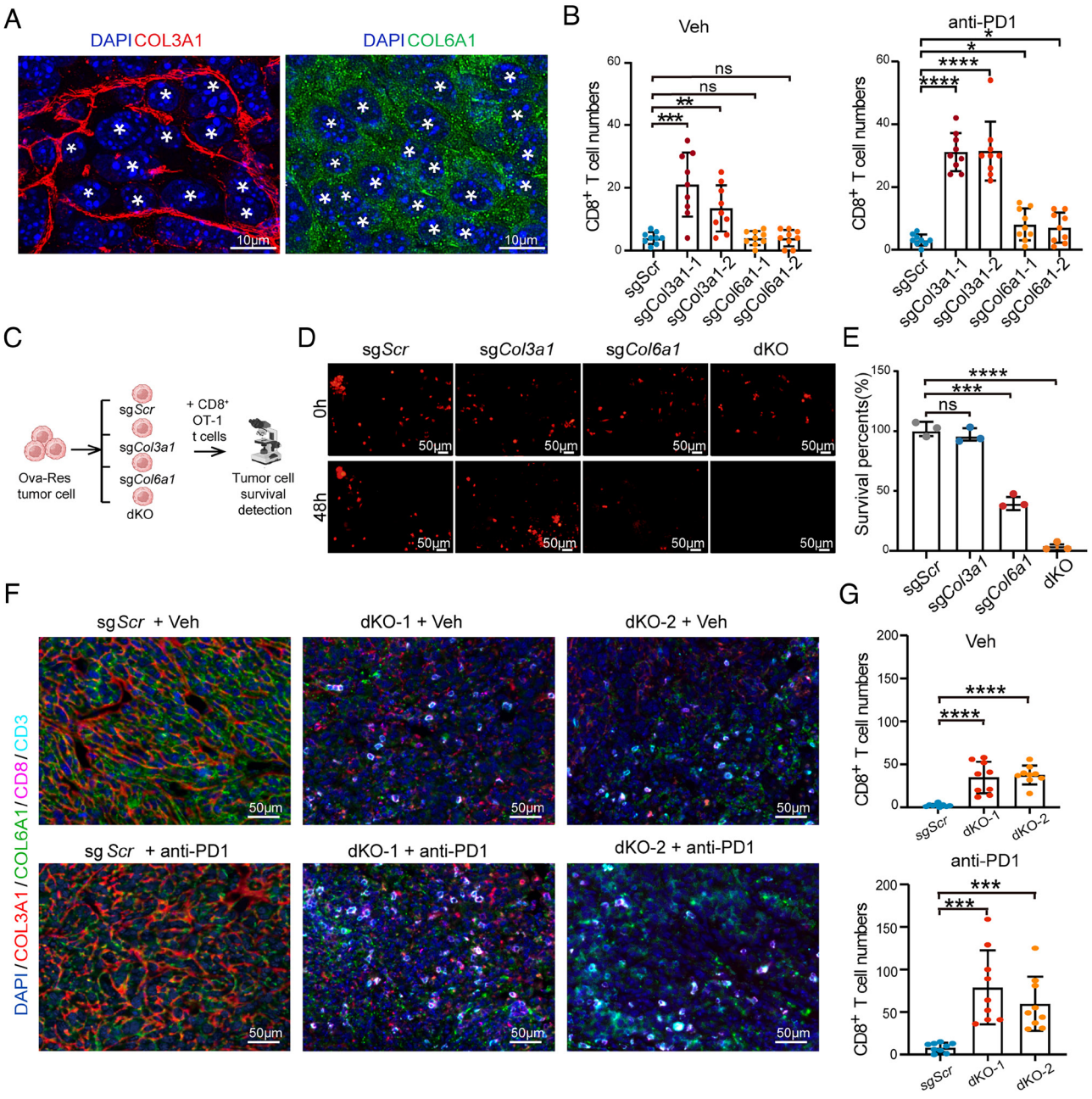

Fig. 5. Col3a1 and Col6a1 prevent T cell infiltration and killing, respectively. (*A*) Representative COL3A1 and COL6A1 staining images of resistant tumors (n = 4 mice). (Scale bar, 10 μm.) (*B*) The bar graphs show the numbers of $CD8^+$ infiltrating T cells in C57BL/6 mice orthotopically transplanted with resistant implanted tumor organoids with sg*Scr*, sg*Col3a1-1/2*, sg*Col6a1-1/2* treated with vehicle (*Left*) or anti-PD1 (*Right*) (independent sections of n = 3 mice). Data presented as mean ± SD. (*C*) Schematic of the resistant-OVA tumor cells with sg*Scr*, sg*Col3a1*, sg*Col6a1*, or dKO cocultured with OT-1 T-cells. (*D*) Representative fluorescence images of resistant-OVA tumor cells with sg*Scr*, sg*Col3a1*, sg*Col6a1*, or dKO cocultured with OT-1 T-cells at 0 and 48 h. (Scale bar, 50 μm.) (*E*) Relative survival percents of resistant-OVA tumor cells with sg*Scr*, sg*Col3a1*, sg*Col6a1*, or dKO cocultured with OT-1 T-cells. Data presented as mean ± SD. (*F*) Representative multiple IHC staining images of COL3A1, COL6A1, CD3, and CD8 in mice orthotopically transplanted resistant implanted tumor organoids with sg*Scr*, dKO-1, or dKO-2 (representative of n = 3 mice) treated with veh (*Top*) and anti-PD1 (*Bottom*). (Scale bar, 50 μm.) (*G*) Bar graphs showing the numbers of $CD8^+$ infiltrating T cells in C57BL/6 mice orthotopically transplanted with resistant implanted tumor organoids with sg*Scr*, dKO-1, or dKO-2 treated with veh (*Up*) and anti-PD1 (*Down*) (independent sections of n = 3 mice). Data presented as mean ± SD. *P* values were calculated using two-tailed Student's *t* test (*B*, *E*, and *G*). ****$P < 0.0001$; ***$P < 0.001$; **$P < 0.01$; *$P < 0.05$. ns, not significant.

treatment, we identified 4 pairs of samples that were collected from the same tissues of the same individuals before treatment and after acquired resistance (10). 3 out of 4 patients had increased expressions of both *COL3A1* and *COL6A1* (Fig. 6*F*). We found that gene signatures upregulated or downregulated in mouse tumors with acquired resistance were significantly positively and negatively, respectively, in the patients acquired resistant to anti-PD1 antibody treatment at all the levels of chromatin accessibility, transcriptome, and proteomics (Fig. 6 *G*–*I* and Dataset S16).

Further, we tested the correlation of these collagen genes with immunotherapy resistance in other types of cancers (27–29). The results showed that melanoma patients, treated with ICI, with high levels of *COL3A1* or *COL6A1*, had shorter overall survival (OS) than those with low levels in both cohorts of GSE78220 and PRJEB23709 (*SI Appendix*, Fig. S8 *D* and *E* and Datasets S17 and S18). Similar results were observed in bladder cancer (*SI Appendix*, Fig. S8*F* and Dataset S19). High expressions of *COL3A1* also predicted poor prognosis in head and neck

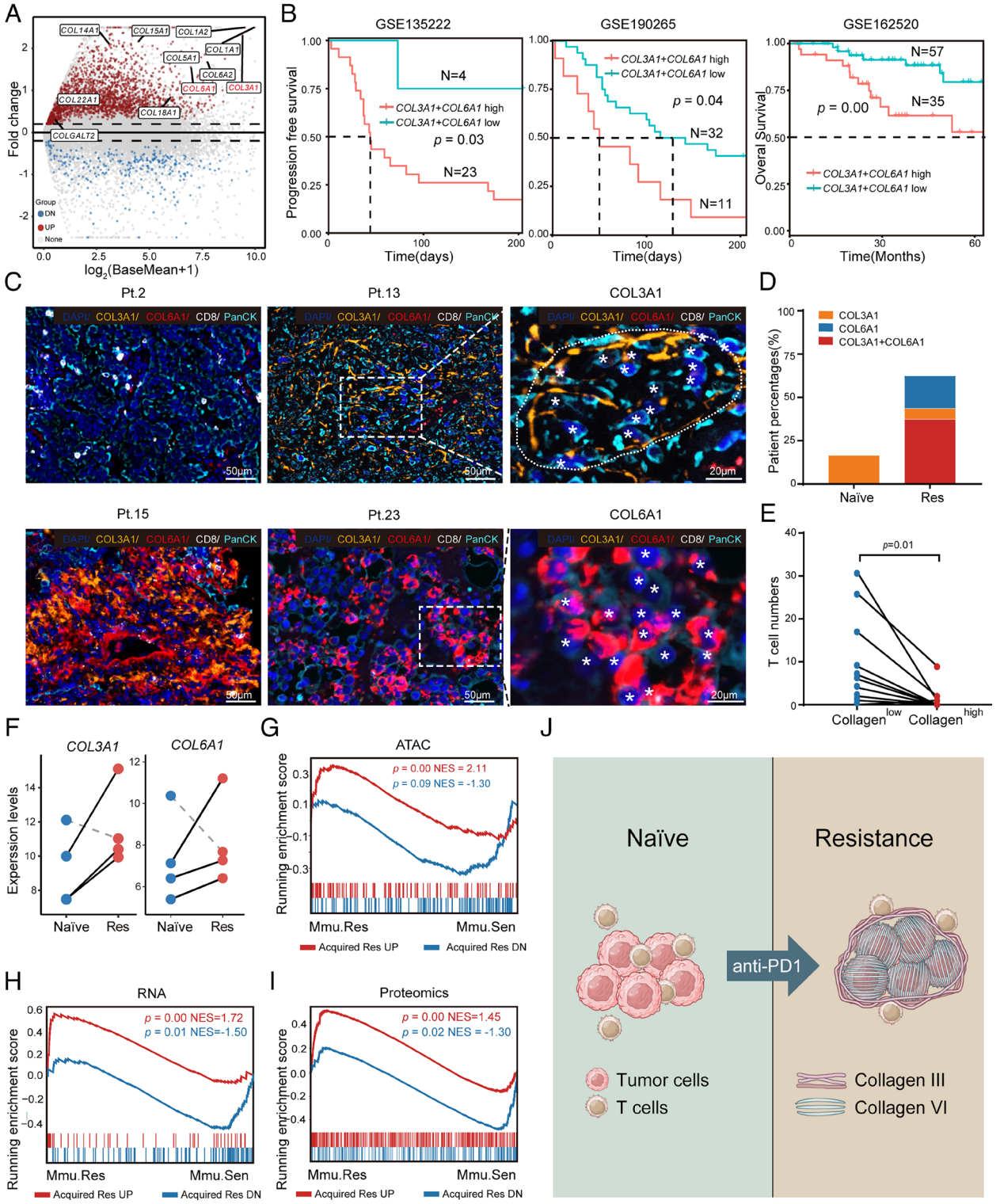

Fig. 6. Collagen layers are associated with AIR in patients. (*A*) Volcano plot showing differentially expressed genes between immunotherapy nonresponsive and responsive NSCLC patients, with a focus on collagen genes. (*B*) Progression-free survival or OS of NSCLC patients under immunotherapy stratified by COL3A1+COL6A1. The *P*-value was calculated by the log-rank test. (*C*) Representative COL3A1, COL6A1, CD8, PanCK multiple IHC staining images in tumors of naïve (Pt.2) and resistant (Pt.13, Pt.15, and Pt.23) patients. (Scale bars, 50, 20 μm.) (*D*) The columns showing the percentages of tumors expressing COL3A1, COL6A1, COL3A1, and COL6A1 in naïve and res patients. (*E*) Dot plots illustrating the $CD8^+$ T cell numbers in tumor areas with low or high Collagen expression. Each line indicated one patient. Two-sided Student's *t* test. (*F*) Dot plots illustrating the expression levels of *COL3A1* and *COL6A1* in naïve and resistant tumors in NSCLC patients from the GSE248249 cohort. Each line indicated one patient. (*G–I*) Gene set enrichment analysis showing enrichment of NSCLC patients with AIR (GSE248249) up- and down-regulated signature genes in mouse resistant tumors at Assay for Transposase-Accessible Chromatin (ATAC) levels (*G*), RNA levels (*H*), and Proteomics levels (*I*). NES, normalized enrichment score. (*J*) Working model for acquired resistance to immunotherapy by cancer cells' self-built physical barriers.

squamous cell carcinoma, though *COL6A1* was not detected (*SI Appendix*, Fig. S8*G* and Dataset S20). These data suggested that the physical barriers formed by collagens might be a general mechanism underlying immunotherapy resistance. Collectively, we found that tumor cells with acquired resistance to immunotherapy expressed high levels of COL3A1 and COL6A1, which formed two physical barriers, a castle-like barrier around a cluster of several tumor cells to prevent T cell infiltration and an armor-like barrier around each individual tumor cell to protect from T cell attack, respectively (Fig. 6*J*).

Discussion

Physical barriers play critical roles in both physiological and pathological conditions (29, 30). In cancers, physical barriers, generally recognized as the nonmalignant cells, mostly the stromal cells, and their ECM, have profound effects on various aspects of tumor (31–35). CAFs and their secreted ECM, together with many other components in the tumor microenvironment, could form physical barriers surrounding the tumor cells, as we observed in immunotherapy sensitive NSCLC, which have been proposed to stimulate the immune response for tumor surveillance. However, tumor progression is associated with ECM remodeling, causing a restriction of immune cell infiltrations and drug delivery in tumors (36–39). Indeed, the features of physical barriers have been applied for clinical diagnosis, such as the broken stromal layers indicating metastatic tumors and the abundance of the stromal layers being associated with poor prognosis (31, 40–42). One of the well-appreciated examples is pancreatic ductal adenocarcinoma (PDAC), in which the fibroblastic stroma can constitute as much as 90% of the whole tumor mass and tightly encompass the tumor cells (43). And consistently, PDAC is notorious for its immune-suppressive TME as refractory to various treatments, including immunotherapy. Here, we describe the physical barriers built by tumor cells themselves. We find that distinct from naïve ones, tumor cells with acquired resistance of immunotherapy express high levels of ECM genes, including COL3A1 and COL6A1, which are generally marker genes of CAFs. These ECM proteins form multiple collagen fibril layers of physical barriers, including the COL3A1-containing castle-like barrier for a cluster of several tumor cells and the COL6A1-containing armor-like barrier for each tumor cell. The castle-like barrier, similar to the stromal barrier, can block the infiltration of the T cells, while the armor-like barrier can directly protect tumor cells from T cell attack (44, 45). Thus, these tumor cell self-built physical barriers, together with other barriers, add additional complexity to the malignant features and significantly contribute to acquired resistance to immunotherapy. Recently, it was proposed that cancer cells could form a second membrane outside of their plasma membrane (46). It would be interesting to test whether these physical barriers and similar ones would be produced by tumor cells themselves in other conditions and their potential functions in tumor progression and response to treatments.

These tumor cell–producing physical barriers consist of COL3A1 and COL6A1-containing collagen fibrils (44, 47–52). There is accumulating evidence suggesting that different collagens could promote tumor progression through distinct mechanisms. In PDAC, tumor cell–expressing Col1a1 homotrimers promote tumor growth and tumor microbiome-associated immune suppression through the α3β1 integrin signaling (53). Depletion of DDR1, a collagen receptor, disrupts collagen fiber alignment and increases the intratumor T cell penetration (36). Collagen III can regulate tumor cell dormancy through the DDR1-STA1 signaling (47). In this study, we propose that COL3A1 and COL6A1, expressed by tumor cells themselves, contribute to the castle-like and armor-like physical barriers, respectively, and provide AIR. It has been shown that collagen can induce $CD8^+$ T cell exhaustion through the LAIR1–SHP-1 axis (54) and COL6A1 can induce T cell autophagic flux via remodeling fibrillar collagen for $CD8^+$ T cell deficiency (44). And consistently, we find that COL3A1 and COL6A1 can prevent T cell infiltration and killing, respectively. Further studies would be required to dissect the detailed shared and distinct mechanisms of these different collagens and the collagen fibrils formed by them on restraining immune cells.

Materials and Methods

Written informed consent of NSCLC patients was obtained from all participants prior to any study procedure. All animal procedures were performed in compliance with the Guide for the Care and Use of Laboratory Animals of Sichuan University and approved by the Animal Care and Use Committee of Sichuan University. Clinical samples, mouse strains, organoid culture, gene editing, cell–cell coculture, animal models, drug treatment, tumor-infiltrating lymphocytes analysis, RNA extraction and RT-qPCR, antibodies and reagents, H/E staining, immunohistochemistry and IF staining, TEM and SEM analysis, MRI imaging and bioluminescent imaging, and bioinformatic and statistical analyses are described in detail in *SI Appendix, Materials and Methods*. This study was approved by the Ethical Research Committee of the West China Hospital (2021-264).

Data, Materials, and Software Availability. Single-cell RNA-seq data, bulk RNA-seq data, and ATAC-seq data have been deposited in the Gene Expression Omnibus (GEO). Specifically, the data are available at GSE261898 (https://www.ncbi.nlm.nih.gov/geo/query/acc.cgi?acc=GSE261898) (55), GSE261889 (https://www.ncbi.nlm.nih.gov/geo/query/acc.cgi?acc=GSE261889) (56), and GSE261597 (https://www.ncbi.nlm.nih.gov/geo/query/acc.cgi?acc=GSE261597) (57). All other data are included in the manuscript and/or supporting information. The authors declare that all scripts used to process data are available from the corresponding author, if requested.

ACKNOWLEDGMENTS. This work was supported by the National Natural Science Foundation of China (82330087; T2221004; 82130007; 82303880; 82170171; 82470188; 82472783; 82300186; and 82300185), the Noncommunicable Chronic Diseases-National Science and Technology Major Project (2023ZD0500500), the Sichuan Science and Technology Program (2023ZYD0057; 2025NSFTD0030; 2025ZNSFSC0047; 2023NSFSC1904; 2025NSFSC1997; 24CXTD05; and 2024NSFSC1699), the China Postdoctoral Science Foundation (2023M732457; 2023TQ0226; 2024T170604; and 2023M732465), the Frontiers Medical Center, Tianfu Jincheng Laboratory Foundation (TFJC2023010004); the 1.3.5. Project for Disciplines of Excellence, West China Hospital, Sichuan University (ZYGD22012), National Clinical Research Center for Geriatrics, West China Hospital, Sichuan University (Z2024JC001), the Post-Doctor Research Project of Sichuan University (JCXK2215 and 2024SCU12033), and the Post-Doctor Research Project, West China Hospital, Sichuan University (2023HXBH018). We sincerely thank Professors Qiang Wei (College of Polymer Science and Engineering, Sichuan University) and Leixiao Yu (National Engineering Research Center for Biomaterials, Sichuan University) for their invaluable technical support and expert guidance.

Author affiliations: [a]Department of Thoracic Oncology, State Key Laboratory of Biotherapy and Cancer Center, West China Hospital, Sichuan University, Chengdu, Sichuan 610041, China; [b]State Key Laboratory of Biotherapy and Cancer Center, West China Hospital, Sichuan University, Chengdu, Sichuan 610041, China; [c]Lung Cancer Treatment Center, West China Hospital, Sichuan University, Chengdu, Sichuan 610041, China; [d]Hospital of Chengdu University of Traditional Chinese Medicine, Chengdu, Sichuan 610072, China; [e]Traditional Chinese Medicine Regulating Metabolic Diseases Key Laboratory of Sichuan Province, Hospital of Chengdu University of Traditional Chinese Medicine, Chengdu, Sichuan 610072, China; [f]Division of Thoracic Tumor Multimodality Treatment Cancer Center, West China Hospital, Sichuan University, Chengdu, Sichuan 610041, China; [g]Chengdu OrganoidMed Medical Laboratory, West China Health Valley, Chengdu, Sichuan 610041, China; [h]Department of Pathology, West China Hospital, Sichuan University, Chengdu, Sichuan 610041, China; [i]Faculty of Medicine, Macau University of Science and Technology, Macau 999078, China; [j]Department of Hematology and Institute of Hematology, State Key Laboratory of Biotherapy and Cancer Center, West China Hospital, Sichuan University, Chengdu, Sichuan 610041, China; [k]Frontiers Medical Center, Tianfu Jincheng Laboratory, Chengdu, Sichuan 610213, China; and [l]Children's Medicine Key Laboratory of Sichuan Province, West China Second Hospital, Sichuan University, Chengdu, Sichuan 610041, China

1. I. Mellman, G. Coukos, G. Dranoff, Cancer immunotherapy comes of age. *Nature* **480**, 480–489 (2011), 10.1038/nature10673.
2. F. Conforti *et al.*, Cancer immunotherapy efficacy and patients' sex: A systematic review and meta-analysis. *Lancet Oncol.* **19**, 737–746 (2018), 10.1016/s1470-2045(18)30261-4.
3. A. Bagaev *et al.*, Conserved pan-cancer microenvironment subtypes predict response to immunotherapy. *Cancer Cell* **39**, 845–865.e7 (2021), 10.1016/j.ccell.2021.04.014.
4. A. Ribas, J. D. Wolchok, Cancer immunotherapy using checkpoint blockade. *Science* **359**, 1350–1355 (2018), 10.1126/science.aar4060.
5. P. Sharma, S. Hu-Lieskovan, J. A. Wargo, A. Ribas, Primary, adaptive, and acquired resistance to cancer immunotherapy. *Cell* **168**, 707–723 (2017), 10.1016/j.cell.2017.01.017.
6. M. D. Vesely, T. Zhang, L. Chen, Resistance mechanisms to anti-PD cancer immunotherapy. *Annu. Rev. Immunol.* **40**, 45–74 (2022), 10.1146/annurev-immunol-070621-030155.
7. N. P. Restifo, M. J. Smyth, A. Snyder, Acquired resistance to immunotherapy and future challenges. *Nat. Rev. Cancer* **16**, 121–126 (2016), 10.1038/nrc.2016.2.
8. S. J. Antonia *et al.*, Four-year survival with nivolumab in patients with previously treated advanced non-small-cell lung cancer: A pooled analysis. *Lancet Oncol.* **20**, 1395–1408 (2019), 10.1016/s1470-2045(19)30407-3.
9. A. J. Schoenfeld, M. D. Hellmann, Acquired resistance to immune checkpoint inhibitors. *Cancer Cell* **37**, 443–455 (2020), 10.1016/j.ccell.2020.03.017.
10. D. Memon *et al.*, Clinical and molecular features of acquired resistance to immunotherapy in non-small cell lung cancer. *Cancer Cell* **42**, 209–224.e9 (2024), 10.1016/j.ccell.2023.12.013.
11. J. S. O'Donnell, M. W. L. Teng, M. J. Smyth, Cancer immunoediting and resistance to T cell-based immunotherapy. *Nat. Rev. Clin. Oncol.* **16**, 151–167 (2019), 10.1038/s41571-018-0142-8.
12. K. Yang, A. Halima, T. A. Chan, Antigen presentation in cancer – mechanisms and clinical implications for immunotherapy. *Nat. Rev. Clin. Oncol.* **20**, 604–623 (2023), 10.1038/s41571-023-00789-4.
13. R. S. Wallis, A. O'Garra, A. Sher, A. Wack, Host-directed immunotherapy of viral and bacterial infections: Past, present and future. *Nat. Rev. Immunol.* **23**, 121–133 (2023), 10.1038/s41577-022-00734-z.
14. N. A. Rizvi *et al.*, Cancer immunology. Mutational landscape determines sensitivity to PD-1 blockade in non-small cell lung cancer. *Science* **348**, 124–128 (2015), 10.1126/science.aaa1348.
15. M. A. Socinski *et al.*, Atezolizumab for first-line treatment of metastatic nonsquamous NSCLC. *N. Engl. J. Med.* **378**, 2288–2301 (2018), 10.1056/NEJMoa1716948.
16. F. Na *et al.*, KMT2C deficiency promotes small cell lung cancer metastasis through DNMT3A-mediated epigenetic reprogramming. *Nat. Cancer* **3**, 753–767 (2022), 10.1038/s43018-022-00361-6.
17. M. Wang *et al.*, Acquired semi-squamatization during chemotherapy suggests differentiation as a therapeutic strategy for bladder cancer. *Cancer Cell* **40**, 1044–1059.e48 (2022), 10.1016/j.ccell.2022.08.010.
18. Z. Lu *et al.*, Dissecting the genetic and microenvironmental factors of gastric tumorigenesis in mice. *Cell Rep.* **41**, 111482 (2022), 10.1016/j.celrep.2022.111482.
19. J. Chen *et al.*, A new type of endometrial cancer models in mice revealing the functional roles of genetic drivers and exploring their susceptibilities. *Adv. Sci. (Weinh)* **10**, e2300383 (2023), 10.1002/advs.202300383.
20. M. Tang *et al.*, The histologic phenotype of lung cancers is associated with transcriptomic features rather than genomic characteristics. *Nat. Commun.* **12**, 7081 (2021), 10.1038/s41467-021-27341-1.
21. H. Jung *et al.*, DNA methylation loss promotes immune evasion of tumors with high mutation and copy number load. *Nat. Commun.* **10**, 4278 (2019), 10.1038/s41467-019-12159-9.
22. H. Raskov, A. Orhan, J. P. Christensen, I. Gögenur, Cytotoxic CD8(+) T cells in cancer and cancer immunotherapy. *Br. J. Cancer* **124**, 359–367 (2021), 10.1038/s41416-020-01048-4.
23. J. R. Conejo-Garcia, Breaking barriers for T cells by targeting the EPHA2/TGF-β/COX-2 axis in pancreatic cancer. *J. Clin. Invest.* **129**, 3521–3523 (2019), 10.1172/jci130316.
24. J. Li, T. Dong, Z. Wu, D. Zhu, H. Gu, The effects of MYC on tumor immunity and immunotherapy. *Cell Death Discov.* **9**, 103 (2023), 10.1038/s41420-023-01403-3.
25. Y. Ni *et al.*, High TGF-β signature predicts immunotherapy resistance in gynecologic cancer patients treated with immune checkpoint inhibition. *npj Precis. Oncol.* **5**, 101 (2021), 10.1038/s41698-021-00242-8.
26. E. Limagne *et al.*, MEK inhibition overcomes chemoimmunotherapy resistance by inducing CXCL10 in cancer cells. *Cancer Cell* **40**, 136–152.e12 (2022), 10.1016/j.ccell.2021.12.009.
27. J. P. Foy *et al.*, Immunologically active phenotype by gene expression profiling is associated with clinical benefit from PD-1/PD-L1 inhibitors in real-world head and neck and lung cancer patients. *Eur. J. Cancer* **174**, 287–298 (2022), 10.1016/j.ejca.2022.06.034.
28. T. N. Gide *et al.*, Distinct immune cell populations define response to anti-PD-1 monotherapy and anti-PD-1/anti-CTLA-4 combined therapy. *Cancer Cell* **35**, 238–255.e6 (2019), 10.1016/j.ccell.2019.01.003.
29. J. K. Mouw, G. Ou, V. M. Weaver, Extracellular matrix assembly: A multiscale deconstruction. *Nat. Rev. Mol. Cell Biol.* **15**, 771–785 (2014), 10.1038/nrm3902.
30. C. Bonnans, J. Chou, Z. Werb, Remodelling the extracellular matrix in development and disease. *Nat. Rev. Mol. Cell Biol.* **15**, 786–801 (2014), 10.1038/nrm3904.
31. J. Winkler, A. Abisoye-Ogunniyan, K. J. Metcalf, Z. Werb, Concepts of extracellular matrix remodelling in tumour progression and metastasis. *Nat. Commun.* **11**, 5120 (2020), 10.1038/s41467-020-18794-x.
32. J. L. Castro, J. T. Erler, Tipping the balance: New insights into stromal regulation of cancer. *Cancer Cell* **40**, 1467–1469 (2022), 10.1016/j.ccell.2022.11.011.
33. T. Stylianopoulos, L. L. Munn, R. K. Jain, Reengineering the physical microenvironment of tumors to improve drug delivery and efficacy: From mathematical modeling to bench to bedside. *Trends Cancer* **4**, 292–319 (2018), 10.1016/j.trecan.2018.02.005.
34. R. Kalluri, The biology and function of fibroblasts in cancer. *Nat. Rev. Cancer* **16**, 582–598 (2016), 10.1038/nrc.2016.73.
35. N. Bansaccal *et al.*, The extracellular matrix dictates regional competence for tumor initiation. *Nature* **623**, 828–835 (2023), 10.1038/s41586-023-06740-y.
36. X. Sun *et al.*, Tumour DDR1 promotes collagen fibre alignment to instigate immune exclusion. *Nature* **599**, 673–678 (2021), 10.1038/s41586-021-04057-2.
37. H. M. Jeon *et al.*, Tissue factor is a critical regulator of radiation therapy-induced glioblastoma remodeling. *Cancer Cell* **41**, 1480–1497.e89 (2023), 10.1016/j.ccell.2023.06.007.
38. A. Kaur *et al.*, Remodeling of the collagen matrix in aging skin promotes melanoma metastasis and affects immune cell motility. *Cancer Discov.* **9**, 64–81 (2019), 10.1158/2159-8290.Cd-18-0193.
39. F. Kai, A. P. Drain, V. M. Weaver, The extracellular matrix modulates the metastatic journey. *Dev. Cell* **49**, 332–346 (2019), 10.1016/j.devcel.2019.03.026.
40. D. R. Welch, D. R. Hurst, Defining the hallmarks of metastasis. *Cancer Res.* **79**, 3011–3027 (2019), 10.1158/0008-5472.Can-19-0458.
41. M. A. Anttila *et al.*, High levels of stromal hyaluronan predict poor disease outcome in epithelial ovarian cancer. *Cancer Res.* **60**, 150–155 (2000).
42. P. Lipponen *et al.*, High stromal hyaluronan level is associated with poor differentiation and metastasis in prostate cancer. *Eur. J. Cancer* **37**, 849–856 (2001), 10.1016/s0959-8049(00)00448-2.
43. A. Neesse *et al.*, Stromal biology and therapy in pancreatic cancer. *Gut* **60**, 861–868 (2011), 10.1136/gut.2010.226092.
44. P. K. Mukherjee *et al.*, Structuring Crohn's disease single-cell RNA sequencing reveals fibroblast heterogeneity and intercellular interactions. *Gastroenterology* **165**, 1180–1196 (2023), 10.1053/j.gastro.2023.07.014.
45. W. Liu *et al.*, Homeoprotein SIX1 compromises antitumor immunity through TGF-β-mediated regulation of collagens. *Cell. Mol. Immunol.* **18**, 2660–2672 (2021), 10.1038/s41423-021-00800-x.
46. T. Yi, G. Wagner, Malignant tumor cells engender second membrane-lined organelles for self-protection and tumor progression. *Proc. Natl. Acad. Sci. U.S.A.* **121**, e2317141121 (2024), 10.1073/pnas.2317141121.
47. J. S. Di Martino *et al.*, A tumor-derived type III collagen-rich ECM niche regulates tumor cell dormancy. *Nat. Cancer* **3**, 90–107 (2022), 10.1038/s43018-021-00291-9.
48. S. Gonçalves-Ribeiro *et al.*, Prediction of pathological response to neoadjuvant treatment in rectal cancer with a two-protein immunohistochemical score derived from stromal gene-profiling. *Ann. Oncol.* **28**, 2160–2168 (2017), 10.1093/annonc/mdx293.
49. B. Su *et al.*, Editorial expression of concern: Let-7d suppresses growth, metastasis, and tumor macrophage infiltration in renal cell carcinoma by targeting *COL3A1* and *CCL7*. *Mol. Cancer* **22**, 74 (2023), 10.1186/s12943-023-01778-y.
50. F. Fernandez-Madrid, R. L. Karvonen, M. J. Kraut, B. Czelusniak, J. W. Ager, Autoimmunity to collagen in human lung cancer. *Cancer Res.* **56**, 121–126 (1996).
51. M. A. Blanco *et al.*, Global secretome analysis identifies novel mediators of bone metastasis. *Cell Res.* **22**, 1339–1355 (2012), 10.1038/cr.2012.89.
52. F. Chen, D. S. Chandrashekar, S. Varambally, C. J. Creighton, Pan-cancer molecular subtypes revealed by mass-spectrometry-based proteomic characterization of more than 500 human cancers. *Nat. Commun.* **10**, 5679 (2019), 10.1038/s41467-019-13528-0.
53. Y. Chen *et al.*, Oncogenic collagen I homotrimers from cancer cells bind to α3β1 integrin and impact tumor microbiome and immunity to promote pancreatic cancer. *Cancer Cell* **40**, 818–834.e19 (2022), 10.1016/j.ccell.2022.06.011.
54. D. H. Peng *et al.*, Collagen promotes anti-PD-1/PD-L1 resistance in cancer through LAIR1-dependent CD8(+) T cell exhaustion. *Nat. Commun.* **11**, 4520 (2020), 10.1038/s41467-020-18298-8.
55. M. Wang *et al.*, Acquired resistance to immunotherapy by physical barriers with cancer cell–expressing collagens in non–small cell lung cancer [scRNAseq]. NCBI GEO. https://www.ncbi.nlm.nih.gov/geo/query/acc.cgi?acc=GSE261898. Deposited 1 February 2025.
56. M. Wang *et al.*, Acquired resistance to immunotherapy by physical barriers with cancer cell–expressing collagens in non–small cell lung cancer [bulk RNAseq]. NCBI GEO. https://www.ncbi.nlm.nih.gov/geo/query/acc.cgi?acc=GSE261889. Deposited 1 February 2025.
57. M. Wang *et al.*, Acquired resistance to immunotherapy by physical barriers with cancer cell–expressing collagens in non–small cell lung cancer [ATACseq]. NCBI GEO. https://www.ncbi.nlm.nih.gov/geo/query/acc.cgi?acc=GSE261597. Deposited 22 May 2025.